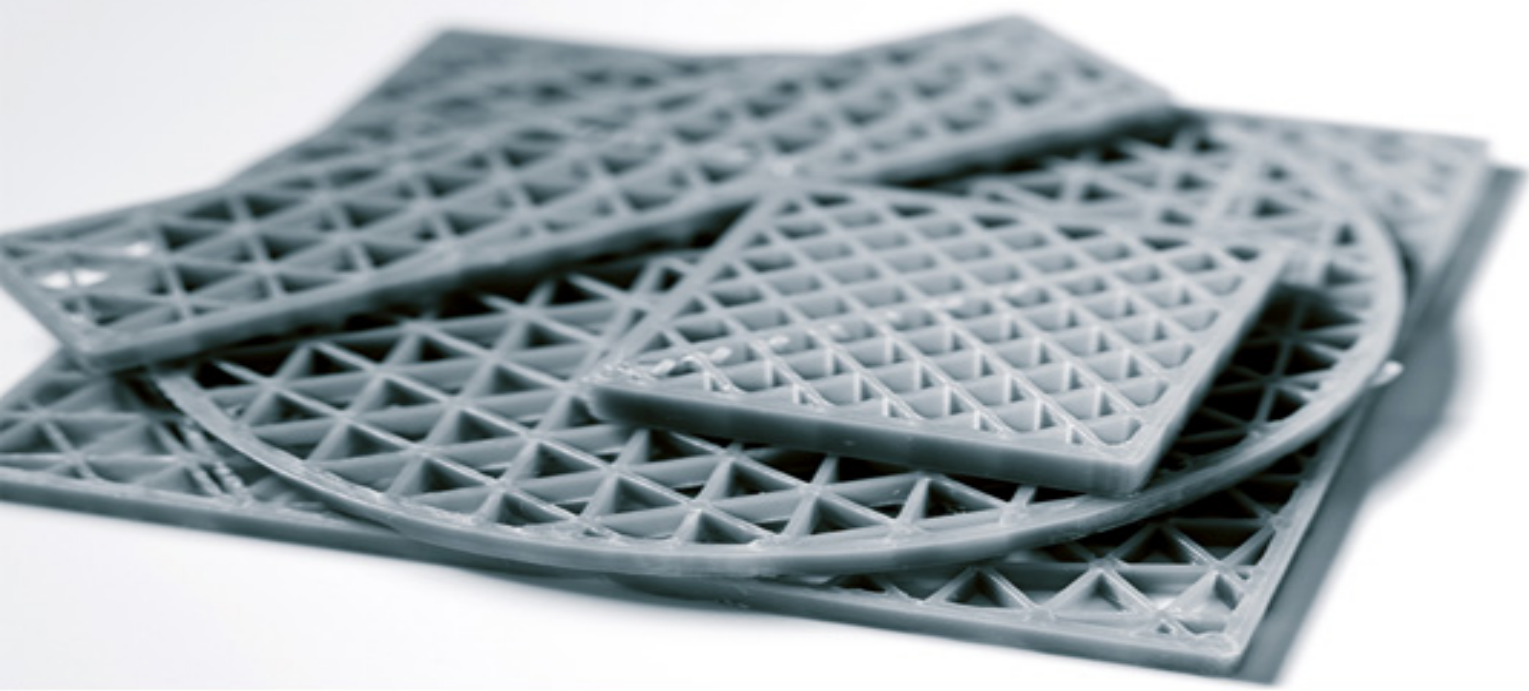


MATERIALS SCIENCE



Light Weight Materials

Processing and Characterization

Edited by
Kaushik Kumar
Bathini Sridhar Babu
J. Paulo Davim

ISTE

WILEY

Table of Contents

[Cover](#)

[Title Page](#)

[Copyright](#)

[Preface](#)

[PART 1 Manufacturing Processing Techniques](#)

[1 Additive Manufacturing: Technology, Materials and Applications in Aerospace](#)

[1.1. Introduction](#)

[1.2. Additive manufacturing configuration](#)

[1.3. Classification of AM technology](#)

[1.4. Materials used in AM technology](#)

[1.5. Aerospace applications of additive manufacturing](#)

[1.6. Challenges faced in the aerospace industry](#)

[1.7. Overcoming aerospace challenges with AM](#)

[1.8. Future work](#)

[1.9. Conclusion](#)

[1.10. References](#)

[1.11. Key terms and definitions](#)

[2 Study of the Manufacturing Process of Polymer Spur Gears: A Light Weight Gear Material](#)

[2.1. Introduction](#)

[2.2. Gear manufacturing process](#)

[2.3. Additive manufacturing/rapid prototyping](#)

[2.4. Laser ablation](#)

[2.5. Hot embossing](#)

2.6. Conclusion

2.7. References

3 Recent Trends in Welding Polymers and Polymer-Metal Hybrid Structures

3.1. Introduction

3.2. Polymer and composites

3.3. Polymerization

3.4. Synthesis of polymer composites

3.5. Types of fillers in composites

3.6. Welding polymers

3.7. Introduction of lightweight metal and alloys

3.8. Welding dissimilar metal alloys

3.9. Industrial application of polymers

3.10. Conclusion

3.11. References

PART 2 Characterization

4 Preparation and Characterization of a Composite Material Using Sisal fibers for Light Body Vehicles

4.1. Introduction

4.2. Literature review

4.3. Materials and methods

4.4. Results and discussion

4.5. Comparison of previous works

4.6. Conclusion and recommendation

4.7. References

5 Optimizing the Polystyrene Catalytic Cracking Process Using Response Surface Methodology

5.1. Introduction

5.2. Material and methods

5.3. Results and discussion

5.4. Conclusion

5.5. References

PART 3 Analysis

6 FEA Comparative Studies on Heat Flux and Thermal Stress Analysis during Conduction Mode and Keyhole Mode in the Laser Beam Welding

6.1. Introduction

6.2. Heat in laser welding

6.3. Modeling

6.4. Results and discussion

6.5. Conclusion

6.6. References

7 Effect of Formability Parameters on Tailor-Welded Blanks of Light Weight Materials

7.1. Introduction

7.2. Experimental procedure

7.3. Results and discussion

7.4. Conclusion

7.5. References

8 Design and Analysis of Sedan Car B-pillar Outer Panel Using Abirbara with S-glass Fiber Hybrid Composites

8.1. Introduction

8.2. Materials and methods

8.3. Composite preparation, testing and analysis

8.4. Design analysis of the B-pillar panel

8.5. Conclusion

[8.6. Recommendations](#)

[8.7. Acknowledgments](#)

[8.8. References](#)

[List of Authors](#)

[Index](#)

[End User License Agreement](#)

List of Illustrations

Chapter 1

[Figure 1.1. Additive manufacturing process \(Tofail 2018\). For a color version of...](#)

[Figure 1.2. Additive manufacturing procedure. For a color version of this figure...](#)

[Figure 1.3. Laser beam melting technology \(Anderl 2014\). For a color version of ...](#)

[Figure 1.4. Electron beam melting \(Mandil, 2016\). For a color version of this fi...](#)

[Figure 1.5. Selective laser melting \(Mumtaz 2008\). For a color version of this f...](#)

[Figure 1.6. Direct metal laser sintering process \(Marrey 2019\). For a color vers...](#)

[Figure 1.7. Laser metal fusion method \(Peyre 2008\). For a color version of this ...](#)

[Figure 1.8. Direct metal deposition process \(Mohamed 2017\). For a color version ...](#)

[Figure 1.9. Aerospace components fabricated through AM \(Hiemenz 2014\)](#)

Chapter 2

[Figure 2.1. Tool-work arrangements in hobbing](#)

[Figure 2.2. An automobile gearbox in which a plastic gear is used as the gear an...](#)

[Figure 2.3. Injection molding setup for fabrication of polymer spur gears \(Sarda...](#)

[Figure 2.4. Fabricated composite spur gears: \(A\). 100% polypropylene \(PP\) and \(B\)...](#)

[Figure 2.5. Types of additive manufacturing of polymer gears](#)

[Figure 2.6. Basic process of hot embossing to manufacture polymer gears](#)

Chapter 3

[Figure 3.1. Two ways of controlled polymerization of CPs \(Verheyen et al. 2017\)](#)

[Figure 3.2a. Polymers produced by linear step-growth polymerization \(Hallenslebe...](#)

[Figure 3.2b. Polymers produced by nonlinear step-growth polymerization \(Hallensl...](#)

[Figure 3.3. Detailed classification of fiber reinforcement used in polymer compo...](#)

[Figure 3.4. \(a\) Effect of percentage addition of Ce on UTS & YTS. \(b\) Effect of ...](#)

[Figure 3.5. Process description of FSW \(Huang et al. 2018b\). For a color version...](#)

[Figure 3.6. Process route of conventional resistance welding of metal and FRP co...](#)

[Figure 3.7. Self-piercing rivet \(SPR\) technique \(Kang et al. 2016\). For a color ...](#)

[Figure 3.8. Plastic/polymer composites used in cars](https://blog.americanchemis...)

Chapter 4

[Figure 4.1. Fabrication approach \(3\)](#)

[Figure 4.2. Flow diagram for fabrication of sisal fiber-reinforced unsaturated p...](#)

[Figure 4.3. Preparation of unsaturated polyester resin \(general purpose resin\) a...](#)

[Figure 4.4. Alkali treatment of sisal fiber protocol](#)

[Figure 4.5. Weight measurement of sodium hydroxide using an analytical precision...](#)

[Figure 4.6. Mixing sodium hydroxide with distilled water. For a color version of...](#)

[Figure 4.7. Sisal fibers immersed in sodium hydroxide solution. For a color vers...](#)

[Figure 4.8. \(a\) Washing process; \(b\) after washing the sisal fibers. For a color...](#)

[Figure 4.9. Local weaving \(loom\) equipment. For a color version of this figure,....](#)

[Figure 4.10. Arranging the fiber using weaving \(loom\) equipment. For a color ver...](#)

[Figure 4.11. Fiber orientation: \(a\) \$0^\circ\$, \(b\) \$\(0^\circ, 90^\circ\)\$, \(c\) \$\pm 45^\circ\$. For a color vers...](#)

[Figure 4.12. Weight measurement of \(a\) \$0^\circ\$ and \(b\) \$\(0, 90\)^\circ\$ fiber orientation. For...](#)

[Figure 4.13. \(a\) Pouring resin; \(b\) pouring hardener. For a color version of thi...](#)

[Figure 4.14. \(a\) Wax/gel; \(b\) mold. For a color version of this figure, see www....](#)

[Figure 4.15. \(a\) Hand lay-up using a normal brush; \(b\) hand lay-up using a roller...](#)

[Figure 4.16. Molding under compression. For a color version of this figure, see ...](#)

[Figure 4.17. Test specimen dimensions: \(a\) tensile test specimen, \(b\) compressio...](#)

[Figure 4.18\(a\). T1 \(47.8 mm × 17.85 mm × 4 mm\) - 0° fiber orientation \(T_{str} = 93 ...](#)

[Figure 4.18\(b\). T2 \(57 mm × 21.15 mm × 4 mm\) - 0° fiber orientation \(T_{str} = 111 ...](#)

[Figure 4.18\(c\). \(a-c\). 0 \(zero\) degree tensile strength test. For a color versio...](#)

[Figure 4.19\(a\). T1\(55 mm × 20 mm × 4 mm\) - \(0,90\)° fiber orientation \(T_{str} = 107 ...](#)

[Figure 4.19\(b\). T2 \(60 mm × 21.3 × 4 mm\) - \(0,90\)° fiber orientation \(T_{str} = 87 ...](#)

[Figure 4.19\(c\). T3 \(60 mm × 20 mm × 4 mm\) - \(0,90\)° fiber orientation \(T_{str} = 10 ...](#)

[Figure 4.20\(a\). T1 \(60 mm × 20.5 mm × 4 mm\) ± 45° fiber orientation \(T_{str} = 39 M...](#)

[Figure 4.20\(b\). T2 \(60 mm × 20.5 mm × 4 mm\) ± 45° fiber orientation \(T_{str} = 35 M...](#)

[Figure 4.21\(a\). C1 \(155 mm × 30 mm × 4 mm\) 0 \(zero\) degree fiber orientation \(Cs...](#)

[Figure 4.21\(b\). C2 \(155 mm × 30 mm × 4 mm\) 0 \(zero\) degree fiber orientation \(Cs...](#)

[Figure 4.21\(c\). C3 \(155 mm × 30 mm × 4 mm\) 0 \(zero\) degree fiber orientation \(Cs...](#)

[Figure 4.22\(a\). C1 \(155 mm × 30 mm × 4 mm\). \(0,90\) degree fiber orientation \(Cstr...](#)

[Figure 4.22\(b\). C2 \(155 mm × 30 mm × 4 mm\) \(0,90\) degree fiber orientation \(Cstr...](#)

[Figure 4.22\(c\). C3 \(155 mm × 30 mm × 4 mm\) \(0,90\) degree fiber orientation \(Cstr...](#)

[Figure 4.23. Variation of tensile strength with fiber orientation For a color ver...](#)

[Figure 4.24. Variation of average tensile strength with fiber orientation. For a...](#)

[Figure 4.25. Young's modulus of elasticity with different fiber orientations. Fo...](#)

[Figure 4.26. Average Young's modulus with different fiber orientations. For a co...](#)

[Figure 4.27. Average flexural strength with different fiber orientation. For a c...](#)

[Figure 4.28. Compressive strength with different fiber orientations. For a color...](#)

[Figure 4.29. Average compressive stress with different fiber orientations. For a...](#)

[Figure 4.30. Analytical precision balance machine. For a color version of this f...](#)

[Figure 4.31. Average weight of dry samples with different fiber orientations. Fo...](#)

[Figure 4.32. Average weight of dry samples. For a color version of this figure,...](#)

[Figure 4.33. Water absorption of different samples. For a color version of this ...](#)

[Figure 4.34. Drafted model of fender using CATIA software: \(a\) all dimension in ...](#)

[Figure 4.35. Prototype of fender. For a color version of this figure, see www.is...](#)

Chapter 5

[Figure 5.1. Schematic illustration of preprocessing of polystyrene. For a color ...](#)

[Figure 5.2. Shredded waste polystyrene with its recycling code 6. For a colorver...](#)

[Figure 5.3. a\) Raw SiO₂-MgO and b\) 950°C calcined silica-magnesium catalyst. For...](#)

[Figure 5.4. Experimental setup of the pyrolysis process. \(a - SS bench-scale pyr...](#)

[Figure 5.5. Thermal degradation of polystyrene obtained from TGA analysis at 10°...](#)

[Figure 5.6. Scanning of raw SiO₂-MgO material with 5 μm magnifications](#)

[Figure 5.7. Scanning of 950°C calcinated silica-magnesium catalyst with 5 μm mag...](#)

[Figure 5.8. EDS spectrum of raw SiO₂-MgO. For a color version of this figure, se...](#)

[Figure 5.9. EDS spectrum of 950°C calcinated silica-magnesium catalyst. For a co...](#)

[Figure 5.10. Comparison plot between experimental and predicted data. For a colo...](#)

[Figure 5.11. Surface plot interaction between C:F and temperature on yield respo...](#)

[Figure 5.12. Surface plot interaction between C:F and time on yield response \(Y\)...](#)

[Figure 5.13. Surface plot interaction between the temperature and the time on th...](#)

[Figure 5.14. Contour plot interaction between the C:F ratio and the temperature ...](#)

[Figure 5.15. Contour plot interaction between the C:F ratio and time on the yiel...](#)

[Figure 5.16. Contour plot interaction between the temperature and time on the yi...](#)

[Figure 5.17. FTIR analysis of silica-magnesium cracking of polystyrene. For a co...](#)

[Figure 5.18. GC-MS analysis of silica-magnesium cracking of polystyrene. For a c...](#)

[Figure 5.19. Effect of C:F ratio on silica-magnesium cracking of polystyrene. Fo...](#)

[Figure 5.20. Effect of the temperature on silica-magnesium cracking of polystyrene...](#)

[Figure 5.21. Effect of time on silica-magnesium cracking of polystyrene. For a c...](#)

Chapter 6

[Figure 6.1. Representation of Kaplan's keyhole model](#)

[Figure 6.2. Geometry of the model. For a color version of this figure, see \[www.ime.unicamp.br/~paulo/...\]\(http://www.ime.unicamp.br/~paulo/...\)](#)

[Figure 6.3. Meshing of the model. For a color version of this figure, see \[www.ime.unicamp.br/~paulo/...\]\(http://www.ime.unicamp.br/~paulo/...\)](#)

[Figure 6.4. Gaussian power distribution. For a color version of this figure, see...](#)

[Figure 6.5. Temperature distributions for various models. For a color version of ...](#)

[Figure 6.6. Comparison of residual stresses in the keyhole model. For a color ve...](#)

[Figure 6.7. Comparison of temperatures in the keyhole model. For a color version...](#)

[Figure 6.8. Thermal results for Gaussian and frustum heat flux. For a color vers...](#)

[Figure 6.9. Stress results for Gaussian and frustum heat flux. For a color vers...](#)

[Figure 6.10. Conduction model for various power inputs. For a color version of t...](#)

[Figure 6.11. Temperature distribution for various power inputs. For a color vers...](#)

[Figure 6.12. Residual stress distribution for various power inputs. For a color ...](#)

Chapter 7

[Figure 7.1. Photographs of the pin profiles of different tools according to N. B...](#)

[Figure 7.2. True stress-true strain curves of 1.4 mm-thick JSC590RN steel sample...](#)

[Figure 7.3. Grid marking of the TWB according to Vijay Gautam et al. For a color...](#)

[Figure 7.4. Tailored Nakazima specimens according to S.M. Chan et al.](#)

[Figure 7.5. Micrographs \(weldable\) of TWBs: \(a\) AA6061, \(b\) AA2014, \(c\) naturall...](#)

[Figure 7.6. Deformed blanks made up of aluminum and SS alloys according to N. Bh...](#)

[Figure 7.7. SEM graphs of the welded zones made of the pin profiles of the SC to...](#)

[Figure 7.8. Al-HSLA welded line moves for three thickness ratios according to Ar...](#)

[Figure 7.9. Welded Al-DP line moves for three thickness ratios according to Arma...](#)

[Figure 7.10. Metallographic images from the welded sample center, according to M...](#)

[Figure 7.11. Investigation of the weld in the transverse direction of similar th...](#)

[Figure 7.12. Effect of the change in thickness by equating standard alloys and d...](#)

[Figure 7.13. FLD developed by dissimilar weld blanks, according to M. Habibi et ...](#)

[Figure 7.14. TWB failure type according to S.M. Chan et al.](#)

[Figure 7.15. Defects observed: \(a\) hot cracks inside the stirred zone; \(b\) view ...](#)

[Figure 7.16. Measures of microstructural and microhardness joints, according to ...](#)

[Figure 7.17. Micrographs showing \(a\) the D1 mixture pattern, \(b\) D1 at the stir ...](#)

[Figure 7.18. SEM images of weld contacts of different alloys: \(a\) D1 and \(b\) D2,...](#)

[Figure 7.19. Fractography of the tensile test specimen: \(a\) Al-Al type weld and ...](#)

[Figure 7.20. Optical cross-section micrographs perpendicular to the frictionstir...](#)

[Figure 7.21. Rotational speed of the tool influences the elongation and FSW plat...](#)

[Figure 7.22. Microhardness survey according to Aruri Devaraju et al. For a color...](#)

[Figure 7.23. Fracture features of dissimilar joints according to Aruri Devaraju ...](#)

[Figure 7.24. Microstructure at optimal process parameters according to Shrinivas...](#)

[Figure 7.25. SEM images of sample no. 2: \(a\) contact zone of AA5083, \(b\) top nug...](#)

[Figure 7.26. Micrographs of weld using the hexagon tool pin profile of different...](#)

Chapter 8

[Figure 8.1. GP polyester resin. For a color version of this figure, see www.iste...](#)

[Figure 8.2. Maximum mold release wax. For a color version of this figure, see ww...](#)

[Figure 8.3. S-glass. For a color version of this figure, see www.iste.co.uk/kuma...](#)

[Figure 8.4. Tensile test. For a color version of this figure, see www.iste.co.uk...](#)

[Figure 8.5. Impact tester. For a color version of this figure, see www.iste.co.u...](#)

[Figure 8.6. Bending test. For a color version of this figure, see www.iste.co.uk...](#)

[Figure 8.7. Compression test. For a color version of this figure, see www.iste.c...](#)

[Figure 8.8. Ethiopian origin stinging nettle plant. For a color version of this ...](#)

[Figure 8.9. Left to right: stem, abirbara fibers before processing and by-produc...](#)

[Figure 8.10. Soaking the fiber in the NaOH solution and drying. For a color vers...](#)

[Figure 8.11. 0°/90° woven preparation. For a color version of this figure, see w...](#)

[Figure 8.12. 0° and/or 90° fiber arrangement. For a color version of this figure...](#)

[Figure 8.13. 0°/90° woven arrangement. For a color version of this figure, see w...](#)

[Figure 8.14. Hand lay-up process. For a color version of this figure, see www.is...](#)

[Figure 8.15. Test machines. For a color version of this figure, see www.iste.co....](#)

[Figure 8.16. Tensile strength of different fiber orientations. For a color versi...](#)

[Figure 8.17. Compression test results for different fiber orientations. For a co...](#)

[Figure 8.18. 0° fiber-oriented bending test result. For a color version of this ...](#)

[Figure 8.19. Bending test comparison. For a color version of this figure, see ww...](#)

[Figure 8.20. Impact test comparison. For a color version of this figure, see www...](#)

[Figure 8.21. Water absorption rate. For a color version of this figure, see www....](#)

[Figure 8.22. Model for the B-pillar and the barrier element. For a color version...](#)

[Figure 8.23. Energy summary graph of the EOSN composite. For a color version of ...](#)

[Figure 8.24. Equivalent stress distribution of the EOSN composite. For a color v...](#)

[Figure 8.25. Energy summary graph of the steel B-pillar outer panel. For a color...](#)

Figure 8.26. Comparison of the deformation between the composite and the steel B...

List of Tables

Chapter 2

Table 2.1. Different manufacturing processes for metal and non-metal gears

Table 2.2. Process parameters for injection molding for different polymer compos...

Chapter 3

Table 3.1. Description of various methods for processing polymer composites (Adv...

Table 3.2. Natural fiber-epoxy composites - mechanical behavior (Jeyapragash et ...

Table 3.3. Polymer welding description (Santos 2009)

Table 3.4. Mechanical performance of cast Mg alloys at room temperature (Song et...

Table 3.5. Properties of low-cost, high-performance cast Mg alloys at room tempe...

Table 3.6. Mechanical properties of various wrought Mg alloys differently proces...

Table 3.7. Designation and description of wrought and cast Al alloys according t...

Table 3.8. Structural material usage in large commercial aircraft (Starke and St...

Table 3.9. Comparison of different materials used in automobiles [http://article...

Chapter 4

Table 4.1. Materials and supplies

Table 4.2. Test results based on the percentage of moisture absorption

Table 4.3. Comparison with previous works on the tensile properties of sisal fib...

Table 4.4. Comparison with previous works on bending properties of sisal fiber c...

Chapter 5

Table 5.1. Atomic composition of raw SiO_2 -MgO versus 950°C calcinated silica-mag...

Table 5.2. Ranges and coded level of process parameters on liquid yield response

Table 5.3. Experimental and predicted response of liquid yield (Y)

Table 5.4. Analysis of variance (ANOVA) for the responses of liquid yield (Y)

Table 5.5. Fit statistical model from ANOVA results for the response of liquid y...

Table 5.6. Physico-chemical analysis of liquid sample with standard diesel prope...

Chapter 7

Table 7.1. Elemental composition

Table 7.2. Properties of standard materials

Chapter 8

Table 8.1. Properties of the designed B-pillar outer panel for different materia...

Table 8.2. Comparison of the steel and EOSN B-pillar outer panels

Light Weight Materials

Processing and Characterization

Edited by

Kaushik Kumar

Bathini Sridhar Babu

J. Paulo Davim

ISTE

WILEY

First published 2021 in Great Britain and the United States by ISTE Ltd and John Wiley & Sons, Inc.

Apart from any fair dealing for the purposes of research or private study, or criticism or review, as permitted under the Copyright, Designs and Patents Act 1988, this publication may only be reproduced, stored or transmitted, in any form or by any means, with the prior permission in writing of the publishers, or in the case of reprographic reproduction in accordance with the terms and licenses issued by the CLA. Enquiries concerning reproduction outside these terms should be sent to the publishers at the undermentioned address:

ISTE Ltd
27-37 St George's Road
London SW19 4EU
UK

www.iste.co.uk

John Wiley & Sons, Inc.
111 River Street
Hoboken, NJ 07030
USA

www.wiley.com

© ISTE Ltd 2021

The rights of Kaushik Kumar, Bathini Sridhar Babu and J. Paulo Davim to be identified as the authors of this work have been asserted by them in accordance with the Copyright, Designs and Patents Act 1988.

Library of Congress Control Number: 2021947485

British Library Cataloguing-in-Publication Data

A CIP record for this book is available from the British Library

ISBN 978-1-78630-797-2

Preface

We would like to present the book *Light Weight Materials: Processing and Characterization*. In the automotive industry, the need to reduce vehicle weight has led to extensive research efforts to develop aluminum and magnesium alloys for structural car body parts. In aerospace, the move towards composite airframe structures has led to an increased use of formable titanium alloys. All of the above-mentioned materials can be categorized into a group called “*lightweight materials*”. The distinguishing feature of lightweight materials is their low densities, ranging from as low as 0.80 g/cm^3 for unfilled polymers to as high as 4.5 g/cm^3 for titanium. Although the density of titanium is higher than that of unfilled polymers, it is significantly lighter than metals: alloy steel (7.86 g/cm^3) and superalloys ($7.8\text{--}9.4\text{ g/cm}^3$). In a nutshell, lightweight materials exhibit a wide range of properties and therefore offer a wide range of applications.

This book primarily aims to provide researchers and students with an overview of the recent advancements in the processing, manufacturing and characterization of lightweight materials, which promises increased flexibility in manufacturing in tandem with mass communication, improved productivity and better quality. It has a collection of chapters contributed by eminent researchers who focus on the topics associated with lightweight materials, including the current buzzword *composite materials*. This book provides the recent advancements in the processing, manufacturing and characterization of lightweight materials and hence would be a panacea in all areas of lightweight materials.

This book has two major objectives. Firstly its chapters by eminent researchers in the field enlighten readers about the current status of the subject. Secondly, as the densities vary a lot so do the applications ranging from automobile, aviation to bio-mechatronics; hence, this book would serve as an excellent guideline for people in all of these fields.

The chapters of this book are divided into three parts, namely [Part 1](#): Manufacturing Processing Techniques, [Part 2](#): Characterization and [Part 3](#): Analysis.

[Part 1](#) contains [Chapters 1–3](#), [Part 2](#) contains [Chapters 4 and 5](#) and [Part 3](#) contains [Chapters 6–8](#).

[Chapter 1](#) explains an advanced technique called *additive manufacturing* (AM), which is predominantly known as 3D printing and rapid prototyping. It is an on-demand production without any dedicated apparatus or tooling, which allows breakthrough performance and supreme flexibility in industries. The aerospace industry is the primary user of AM, as it enables it to create complex user-defined part design and fabricate with different lightweight materials without wastage of raw materials, reducing the time and cost of production. This chapter provides in-depth knowledge about its classification and selection process for various applications required by engineering industries, especially in the aerospace industry.

[Chapter 2](#) mainly deals with the manufacturing of polymer gears. Polymer gears are widely used in medical devices upon which human lives depend. In addition, they are useful in other applications such as in the automotive and manufacturing industries. A precise gear of better design and effective manufacturing process decides its long-term application, strength and property. Polymer gears can be fabricated with the same machining process as metal gears, usually milling or hobbing from a blank. However, for lightweight materials, such as polymers, it is preferable

to be either fabricated by injection molding or machined from a rod (additive manufacturing). The details of such manufacturing techniques are presented in this chapter.

[Chapter 3](#), the last chapter of [Part 1](#), discusses in detail reinforcing, performance analysis, processing and characterization of various methods of polymer welding, i.e. laser welding, infrared welding, spin welding, stir welding, and vibration welding. This chapter also covers various alloys of aluminum for lightweight applications and the current status of polymer composite applications in industries and future prospects. This chapter highlights the complications related to fusion, heat transfer and joint strength, as well as their solutions with the future prospect of polymer welding empowering polymers to be an absolute substitute for metal, which can be achieved by understanding the concept of dissimilar welding for joining polymer composites with metals and their controlling factors, and by selecting an appropriate welding process for various types of polymers.

[Chapter 4](#), the first chapter of [Part 2](#), provides the reader with an idea of fabrication and a description of the processing techniques of natural-based composites for light body vehicle applications. In doing so, the genetic equation for modeling tool flank wear is developed using experimentally measured flank wear values and genetic programming. Using these results, the genetic model presenting the connection between cutting parameters and tool flank wear is extracted. Then, based on a defined machining performance index and the obtained genetic equation, optimum cutting parameters are determined. This chapter concludes that the proposed modeling and optimization methodology offer the optimum cutting parameters and can be implemented in real industrial applications.

[Chapter 5](#) presents the response surface methodology, an optimization technique, to design a catalytic cracking experiment of plastic waste. The catalyst-to-feedstock ratio, the operating temperature and the reaction time were chosen as an effective parameter of the catalytic cracking process. The characterization of the obtained liquid product was performed using the Fourier transform with infrared (FTIR) spectra, gas chromatography with mass spectrometry (GC/MS) analysis and physico-chemical analysis. This chapter concludes that the developed quadratic model is well fit to the experimental domains and predicts operating conditions that are most suitable for conducting catalytic cracking experiments under recycling techniques of lightweight materials, especially plastics.

[Chapter 6](#), the first chapter of [Part 3](#), discusses laser welding. The uniqueness of this chapter is the way it has dealt with the subject. The finite element analysis was used to select suitable models for the Gaussian beam profile and the application of the Frustum model to conduction mode welding and keyhole laser welds. Temperature and stress analysis was carried out within and around the weld region. This chapter discusses the analytical comparative approximation of different model approaches applicable to the laser weld process, and indicates that the parametric study information will be useful to the engineers of nuclear fabrication applications in finalizing different components.

[Chapter 7](#) elaborates on the effect of formability parameters on tailor-welded blanks of lightweight materials. The product finds its maximum application in the automotive manufacturing industry. It is quite common that different materials with varying cross-sections are used based on the requirements in aerospace and automotive industries. To manage the herculean task of organizing this, researchers have enthusiastically proposed a tailor-made welded blanks (TWB) strategy, and in many

automotive industries this technique has been adopted. This chapter suggests testing the formability of tailor-welded blanks with various light alloy sheets used in the aerospace and automotive industries. An overall review of various parameters that affect the formability of tailor-welded blanks is presented in this chapter, so that other investigators can rely on the same for more critical observations in this field.

Chapter 8, the last chapter of this section, presents the various ways of optimizing a vehicle body, such as shape optimization for aerodynamics and aesthetics, and weight of materials to be used for fuel efficiency, material conservation, recyclability and others. This chapter considers a product called “B-pillar”, one of the critical structural support members of sedan cars. They have replaced the existing material with a composite, mainly to overcome the stress developed due to the system as it is a structural member and to safeguard the occupant in the case of a side crash. Different mechanical properties such as tensile, compression and bending strength, as well as water absorption, were measured. The model of the sedan car B-pillar panel developed was analyzed for impact and crush simulation. It concluded that a composite can be used for the outer panel of B-pillar, which results in reduced vehicle weight and fuel consumption and increased energy absorption.

First and foremost, we would like to thank God. It was your blessing that provided us with the strength to believe in passion and hard work and to pursue our dreams. We thank our families for having the patience with us for taking yet another challenge that decreased the amount of time we could spend with them. They are our inspiration and motivation. We would like to thank our parents and grandparents for allowing us to follow our ambitions. We would like to thank all the contributing authors, as they are

the pillars of this structure. We would also like to thank them for believing in us. We would like to thank all of our colleagues and friends in different parts of the world for sharing their ideas helping us to shape our thoughts. We will be satisfied with our efforts when the professionals concerned with all the fields related to lightweight materials are benefitted.

We owe a huge thanks to all of our technical reviewers, Editorial Advisory Board members, Book Development Editor and the team at ISTE Ltd for their availability to work on this huge project. All of their efforts helped us to complete this book, and we could not have done it without them.

Last, but definitely not least, we would like to thank all of the individuals who have taken time out and helped us during the process of editing this book. Without their support and encouragement, we would have probably given up the project.

Kaushik KUMAR
Bathini SRIDHAR BABU
J. Paulo DAVIM
September 2020

PART 1

Manufacturing Processing

Techniques

1

Additive Manufacturing: Technology, Materials and Applications in Aerospace

Additive manufacturing (AM), predominantly known as 3D printing, is transmuting product design, production and service. AM assists us in achieving on-demand production without dedicated apparatus or tooling, unlocks digital design tools, and leads to breakthrough performance and supreme flexibility in industries. Knowledge acts as a barrier to this technique since the selection process for various materials and their applications and requirements differ from each individualized processes. The aerospace industry is the primary user of AM, as it enables it to create complex user-defined part design and fabricate with different materials without wastage of raw materials, reducing the time and cost of production.

This research work promotes the clarity of AM technology by providing in-depth knowledge about its classification and selection process for various applications required by engineering industries, especially in the aerospace industry. Several 3D printing methods and the use of different materials and their applications in the aerospace industry are discussed in detail.

1.1. Introduction

Additive manufacturing technology enables a variety of innovative and economically reliable components when compared to conventional manufacturing methods. The term “rapid prototyping” (RP) is defined as the emphasis of

generating a design for a prototype or a base model at a faster rate to promote the end product for manufacturing. It is used in various industries to rapidly develop various peripherals with intricate user-defined models into a commercialized product (Devadiga 2017). RP technology emerged as the first methodology for making user-defined models, but it lags behind modern methodology due to its inadequate efficiency to effectively create products within the time limit and cost of production. Additive manufacturing (AM) technology developed from RP technology to enhance the quality of the output product. AM acts as a basic principle of creating three-dimensional (3D) objects generated through computer-aided design (CAD) systems. In AM technology, the components are produced from CAD data and slicing software to create a specified part geometry rather than complex tooling and additional fixtures that are used in conventional manufacturing methodologies. In AM technology, the structures are built in a layer-by-layer fashion with a specified cross-section, which is not only used in manufacturing industries to fabricate automobile components and dynamic mechanical structures but is also used in tissue engineering with the capacity of bioprinting to create biomedical implants, artificial human organs and drug delivery systems (Herzog 2016). AM technology acts as a key to solving environmental and engineering issues since it has free-form fabrication (FFF) that facilitates producing user-defined geometries with all classes of raw materials without any limitations, unlike metals, non-metals, alloys and synthetic polymers, with no wastage of materials. This technology can be further improved by increasing its applications across the engineering industry (Dhinakaran 2019). There are numerous stages involved in product development, initially from generating a CAD model to the conversion of the STL file format to make the end product (DebRoy 2018). As AM is a multi-purpose

method, it is used not only for producing new components but also to simplify and alter the existing components.

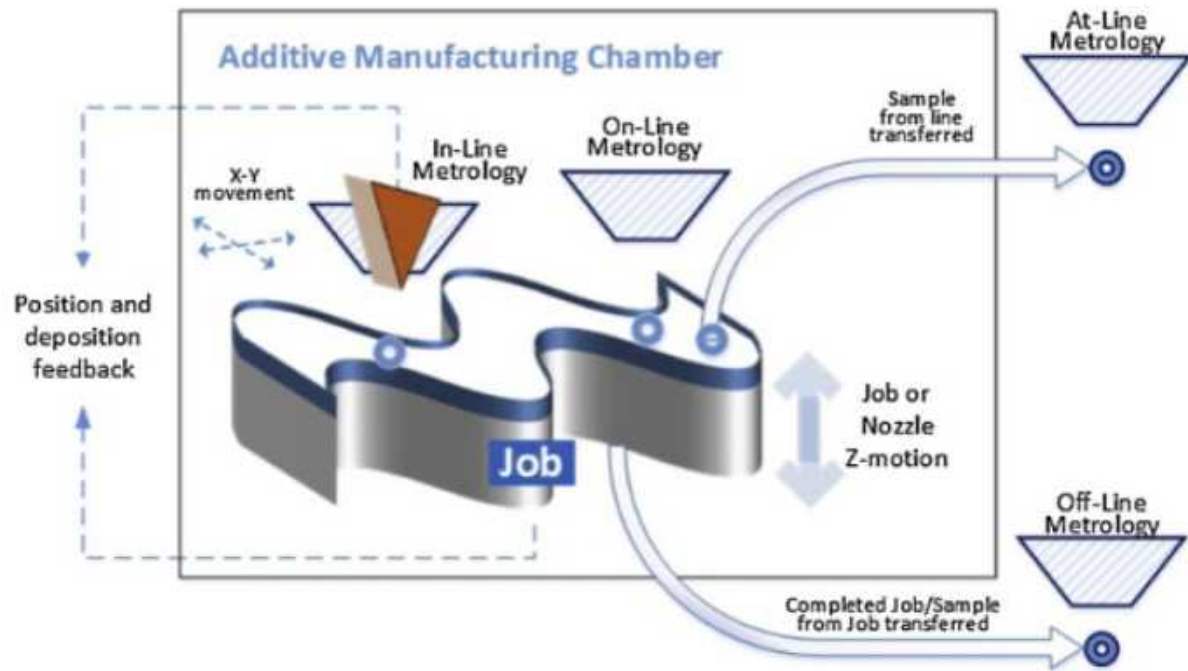


Figure 1.1. Additive manufacturing process (Tofail 2018). For a color version of this figure, see www.iste.co.uk/kumar/materials.zip

1.2. Additive manufacturing configuration

AM technology uses specialized designing software to produce CAD models with user-defined cross-sections and process constraints such as material restraints, source of energy, timings and layer thickness. The computed CAD design is then formatted into an STL (stereolithographic) file format. The STL file displays the peripherally closed external surface of the CAD geometry and performs the slice calculation using a slicing software, and then it is sent to the AM machine which is verified for its build orientation and position (Brandsmeier 2017). The construction of the

material is automatically carried out in a layered fashion by the machine (3D printer) without any human supervision. The 3D printer needs manpower to only monitor the availability of raw materials and to check for any run-time errors. After completing the product, the interaction of the part with the machine is cut down by adjusting the machine temperature and then detached. In post-processing, the part is cleaned before use and treated mechanically for surface finish and the required texture (Scheck 2016).

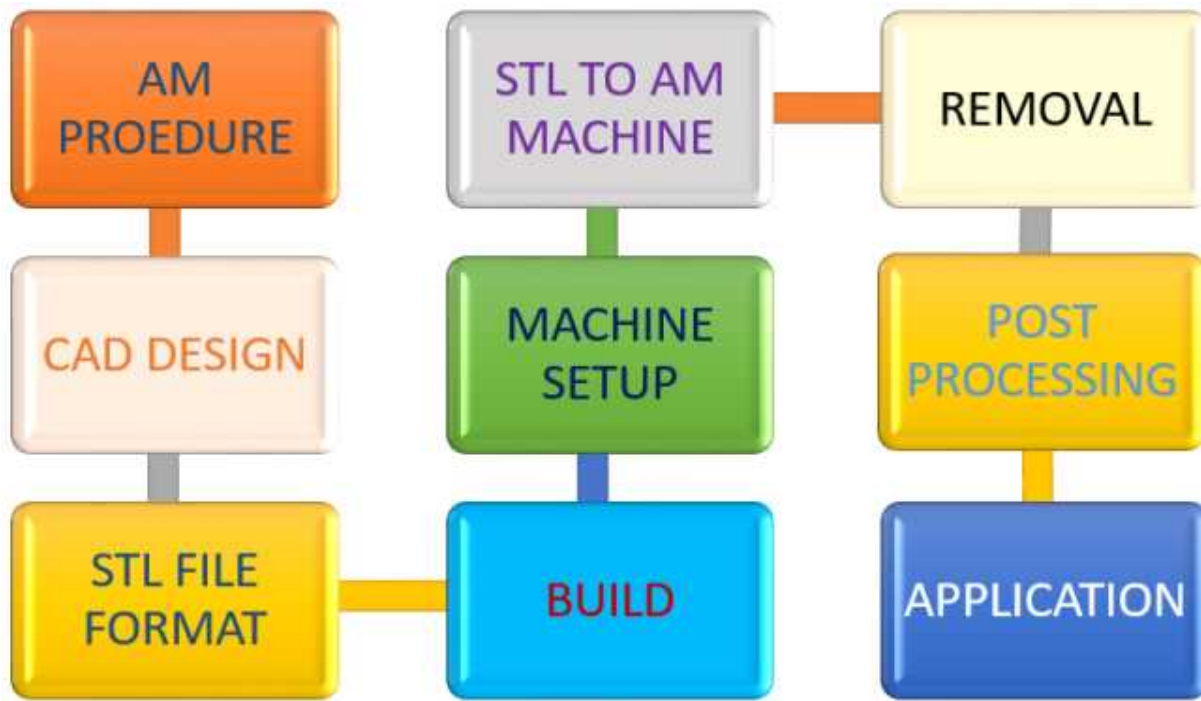


Figure 1.2. Additive manufacturing procedure. For a color version of this figure, see www.iste.co.uk/kumar/materials.zip

1.3. Classification of AM technology

The diversity of materials has convoluted the 3D structures being fabricated with a distinct class of functional time and assembly. AM technology emerged as a great boon over conventional methodologies for creating complex